THE ASTROPHYSICAL JOURNAL, 406:482–488, 1993 April 1

MICROARCSECOND PROPER MOTIONS OF EXTRAGALACTIC WATER VAPOR MASERS IN M33

L. J. GREENHILL, J. M. MORAN, M. J. REID, AND K. M. MENTEN
Harvard-Smithsonian Center for Astrophysics, 60 Garden Street, Cambridge, MA 02138

AND

H. HIRABAYASHI[1]
Nobeyama Radio Observatory, Nobeyama, Minamisaku, Nagano 384-13, Japan
Received 1992 April 30; accepted 1992 October 1

ABSTRACT

We present a second-epoch spectral line VLBI synthesis map of the H_2O maser associated with the H II region IC 133 in the galaxy M33. This map is about 2.5 times more sensitive than the earlier one. Thirty-two spatially distinct maser features have been identified, and we have discovered a second center of maser activity within the IC 133 complex, IC 133 West, which is displaced $\approx 0\farcs3$ (1 pc at a nominal distance of 720 kpc) from IC 133 Main. The most blueshifted maser features are located in IC 133 West, which may mark the location of a separate star forming region.

Comparing the two available maps of IC 133, we have estimated the right ascension components of proper motion over a period of 479 days for five maser features to accuracies of between 7 and 16 μas. The dispersions in transverse and radial velocities for the maser features are consistent with the accepted distance to M33 of 720 kpc, where the data admit a fractional uncertainty in distance of 50%. Our result represents the first successful measurements of proper motions in an extragalactic H_2O maser source and demonstrate the feasibility of making such measurements in other galaxies. Improvements in this technique may make it important for the estimation of extragalactic distances.

Subject headings: astrometry — galaxies: ISM — galaxies: individual (M33) — H II regions — ISM: individual (IC 133) — masers

1. INTRODUCTION

Spectral line VLBI studies of H_2O maser proper motions have yielded distance estimates for the Galactic Center and six star-forming regions in our Galaxy: the Orion Kleinmann-Low (KL) nebula, W51 Main, W51 North, Sgr B2 North, Sgr B2 Middle, and W49N (see summary in Greenhill et al. 1990). Distance measurements that rely on maser proper motions are of particular importance since they are independent of the calibrations that are commonly employed in conventional extragalactic distance estimates (e.g., extinction and metallicity). Proper motions can be measured by tracking the relative positions of the maser features with spectral line VLBI observations, at several epochs spread over months to years (limited by the lifetime of each individual maser feature). The proper motions, when combined with relative positions and line-of-sight (radial) velocities, can be used to analyze the three-dimensional dynamics of the region containing the masers (e.g., outflow) and to estimate the distance to the maser source (Reid & Moran 1988).

In principle, the estimation of distances via the measurement of H_2O maser proper motions can be extended to extragalactic maser sources, of which there are several known within 3 Mpc that are observable from the northern hemisphere (Greenhill et al. 1990). Current ground-based VLBI arrays, which can have a maximum resolution of ~ 200 μas, are capable of discerning proper motions for sufficiently strong masers that lie within a few Mpc, depending on source structure (Reid, Moran, & Gwinn 1987). A transverse motion of 1 km s^{-1} at a distance of 1 kpc results in a proper motion of 210 μas. Hence, for Galactic sources, the velocities of H_2O masers, which are typically tens of km s^{-1}, correspond to proper motions of at least a few milliarcseconds per year (mas yr^{-1}) while for M33 (720 kpc), a transverse motion of 30 km s^{-1} corresponds to only about 10 μas yr^{-1}. Interpreting these minute motions for extragalactic sources is complicated by the difficulty of obtaining corroborative measurements of quantities such as the systematic velocity of the source, which are useful in interpreting the dynamics of the region.

Greenhill et al. (1990) presented the first VLBI maps of an extragalactic H_2O maser, the maser associated with the H II complex known as IC 133, in the nearby galaxy M33. The VLBI image of IC 133 showed that the maser components were spread irregularly over 30 mas (~ 0.1 pc), at the 1987 June epoch of observation. The angular extent of the source, and the flux density and characteristic clustering of the maser features would be similar to those of the most luminous Galactic H_2O maser, the one in W49N (Walker, Matsakis, & Garcia-Barreto 1982), were it at a distance of 720 kpc.

Some properties of the thermal continuum emission of the IC 133 H II complex are typical of massive star forming regions in our Galaxy (Greenhill et al. 1990 and references therein). For example, the estimated total luminosity, at least 10^7 $L_\odot$ (Israel et al. 1990), is comparable to that of the W49 and W51 regions. However, unlike these sources, IC 133 has a dearth of 21 cm H I emission, relative to infrared continuum emission (Rice et al. 1990). Israel et al. (1990), who may have detected 2 μm vibrationally excited H_2 emission associated with IC 133, conclude that despite its prominent maser activity and presumed youth (5×10^6 yr), IC 133 is poor in gas and dust on scales of 100 pc.

In this paper, we report a second successful VLBI experiment on the IC 133 extragalactic H_2O maser in M33. The

[1] Currently at the Institute of Space and Astronautical Sciences, 3-1-1 Yoshinodai, Sagamihara, Kanagawa 229, Japan.

sensitivity of our new observations surpasses that of the previous ones by almost a factor of 3. With this higher sensitivity we have been able to identify more than twice the number of maser features detected before. By comparing the positions of features detected in both epochs, we are able for the first time to measure relative proper motions in an extragalactic H_2O maser source. This result is important because it demonstrates the feasibility of such measurements, which can eventually be used to estimate extragalactic distances.

2. VLBI OBSERVATIONS

The Mark III VLBI observations of the H_2O maser in IC 133 were made on 1988 September 25 and 26, from about 23:00 UT to 16:00 UT. The six stations (Max-Planck-Institut für Radioastronomie 100 m, Haystack Observatory, NRAO 140 foot [43 m],[2] NRAO VLA, Owens Valley Radio Observatory 130 foot [40 m], and Nobeyama Radio Observatory 45 m) whose parameters are listed in Table 1 comprised the array. In an effort to minimize the impact of systematic errors on the proper motions, the arrangement of observations, choice of calibration sources, and the setup of the Mark III terminals were nearly identical to those used in the previous observations (Greenhill et al. 1990).

We recorded a total of about 86 baseline-hours of data, 62% of which were used to observe IC 133. Three 2 MHz video bands were centered at -216.28, -240.35, and -264.43 km s^{-1} with respect to the local standard of rest (LSR). Each video converter was assigned to an individual RF bandpass for the duration of the experiment, so that instrumental delay and phase parameters were easily calibrated using the observations of the calibration sources. The automatic Mark III phase calibration system was not used because nonstandard local oscillator frequencies were required to position the spectra in the bandpasses.

3. DATA REDUCTION

Details of the correlation, calibration, and synthesis imaging are presented by Greenhill (1990) and are similar to those described by Greenhill et al. (1990). The absolute flux density calibration is uncertain by 25%. For each station we determined the clock drift rates to better than 0.2 ps s^{-1} (8.6 ns day^{-1}) and the clock offsets to better than 4 ns, for each video converter. Note that at each station the video converters have independent offsets, differing by up to $\sim$30 ns. The electronic phase offsets of the video converters for each station were measured to an accuracy of about 10°.

We phase referenced the spectral line data on IC 133 to reduce the effects of the atmosphere and systematic errors (Thompson, Moran, & Swenson 1986). The "reference" channel was at $V_{LSR} = -210.03$ km s^{-1}, near the peak in the maser emission. We were constrained in our choice of reference because of the requirement that it be sufficiently strong ($\sim$2 Jy) to be detected on most baselines within the coherence time, which is a few minutes at 22 GHz.

Systematic delay errors in phase referenced data induce second-order position errors in synthesized images. For a maser feature that lies in the "reference" band, the position error is proportional to the difference in video frequency between the feature and reference channel. For a feature in another (remote), band, the error is proportional to the root-sum-square of the difference in video frequency between the reference channel and its band center, and the remote feature and its band center. For remote bands the more complex functional dependence on frequency arises because of the independent delay errors among bands. We have assumed that systematic delay errors are uncorrelated between bands and can be approximated as statistical errors. In addition, the uncertainty in the instrumental phase offset between remote and reference bands (i.e., between video converters) misaligns the coordinate origins of maps from different bands. However, other systematic errors, such as an inaccurate astrometric position for emission from the reference channel, may be the same at each epoch, and do not strongly affect proper motions, if the (u, v)-tracks are similar. Such errors are neglected here.

The proportionality between frequency and position error was determined by a Monte Carlo simulation. Visibility data for an isolated maser spot were perturbed by adding Gaussian random fluctuations in phase, as prescribed by known phase and delay calibration uncertainties, and Fourier transformed into an image, the process being repeated many times. The proportionality should be a function of the calibration uncertainties and the distribution of data in the (u, v)-plane. From this simulation, the 1 σ systematic position errors were estimated to be $\sim$0.13 and 0.57 μas km^{-1} s or $\sim$1.8 and 7.7 μas MHz^{-1} in right ascension and declination, respectively. The phase calibration errors cause the origins of the three bands to have uncertainty in alignment of 11 and 49 μas (1 σ) in right ascension and declination, respectively. The magnitude of this misalignment does not affect the proper motions since none were associated with features in a remote band (see § 5.1.). For the reference band of the previous, less sensitive experiment, the 1 σ systematic position errors are $\sim$0.59 and 2.5 μas km^{-1} s or $\sim$8.0 and 34.5 μas MHz^{-1} in right ascension and declination, respectively.

[2] The NRAO is operated by Associated Universities, Inc., under cooperative agreement with the National Science Foundation.

TABLE 1

VLBI NETWORK: TECHNICAL DETAILS AND PERFORMANCE

Station Designation[a]	Receiver Type	Feed Polarization	Diameter (m)	T_{sys}[b] (Jy)	Amount of Useful Data (hr)
MPI	Maser	Linear	100	100	3.3
Haystack	Maser	LCP	37	750	3.4
NRAO	Maser	LCP	43	600	2.6
VLA	HEMT	LCP	27 × 25[c]	100	3.6
OVRO	Maser	LCP	40	300	3.6
NRO	HEMT	LCP	45	650	1.7

[a] MPI: Max-Planck-Institut für Radioastronomie, Effelsberg, Germany. Haystack: Haystack Observatory, Westford, MA. NRAO: National Radio Astronomy Observatory, Green Bank, WV. VLA: Very Large Array, Socorro, NM. OVRO: Owens Valley Radio Observatory, Big Pine, CA. NRO: Nobeyama Radio Observatory, Nobeyama, Japan.

[b] Characteristic system temperatures at about 45° elevation. For each station, the value is the system temperature multiplied by the sensitivity of the telescope in units of Jy K^{-1}. The absolute scale is uncertain by $\sim$25%.

[c] Phased array in its smallest, D, configuration. The equivalent geometric diameter was 130 m.

4. RESULTS

A total of 34 baseline-hr of amplitude and phase-calibrated data were obtained in good weather on 11 baselines between 23:30 and 14:40 UT on 1988 September 25 and 26, respectively. The longest useful baseline, NRO-VLA, was 8771 km, while the shortest, OVRO-VLA, was 1026 km. The longest

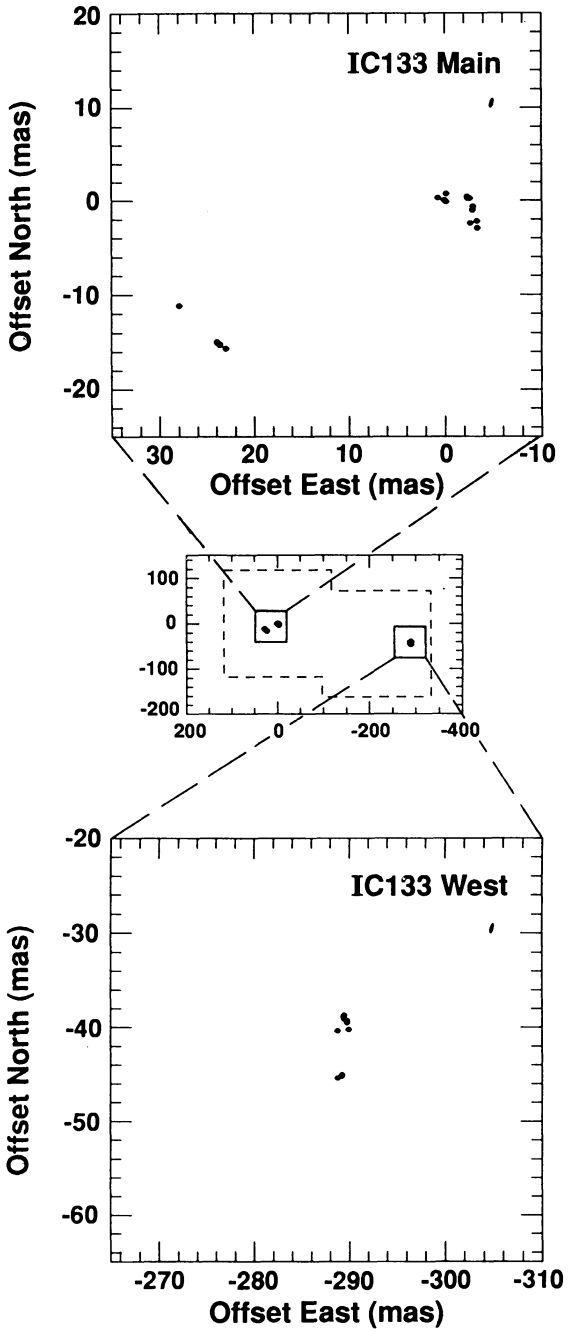

FIG. 1.—VLBI maps of IC 133 for the second epoch. *Center*: An overview of IC 133 that shows the relative positions of IC 133 Main and IC 133 West. The dashed box indicates the region searched for emission. *Top*: An expanded view of IC 133 Main. Each maser feature is denoted by a filled circle. The FWHM of the synthesized beam is shown in the northwest corner. *Bottom*: An expanded view of IC 133 West. The celestial coordinates of the origin are $\alpha_{2000} = 01^h33^m16^s.545 \pm 0^s.008$, $\delta_{2000} = 30°52'50''.0 \pm 0''.1$. At the assumed distance of 720 kpc, 1 mas corresponds to 0.003 pc.

baselines, those linking NRO with Haystack and NRAO, were not sufficiently sensitive to be useful.

To search for emission not observed previously, we imaged the IC 133 region at low angular resolution in an approximately rectangular field measuring 450 × 195 mas in right ascension and declination respectively (Fig. 1). The field included the reference feature and a position ~0".3 west at which Greenhill et al. (1990) reported a marginal VLA detection of blueshifted maser emission. Based on the results of this low angular resolution search, we imaged three smaller fields (20.5 × 20.5 mas) at high resolution. The FWHM of the primary lobe of the untapered interferometer beam was 0.26 × 0.95 mas at a position angle of −14° east of north. The 1 σ noise level, ~4 mJy in a 0.48 km s^{-1} wide spectral channel, was consistent with that expected theoretically, from antenna and receiver performance characteristics. The sensitivity of these images exceeded those of the first epoch by a factor of about 2.5 and of the search for emission by about a factor of 2.

The positions of emissions that lie in contiguous spectral channels and are spatially associated were averaged to provide the positions of the spatially distinct maser features, which can correspond to individual spectral features. The uncertainties in these averaged positions include random errors, due to finite signal-to-noise ratio (SNR) and systematic position errors, which are highly correlated among frequency channels and undiminished by the averaging. Thirty-two maser features were detected, clustered on three different size scales of order 1, 5, and 20 mas. Figure 1 shows a map of these features in IC 133 and Table 2 summarizes their relative positions. We found a second distinct center of maser activity within the IC 133 complex, IC 133 West, which is displaced ~0".3 (1 pc at a distance of 720 kpc) from the reference feature in IC 133 Main. Such multiple structure is similar to that found toward numerous star-forming regions in the Milky Way, many of which host maser activity separated from each other by 0.1 pc to several pc. Examples include W49N and W49S, W51 Main, North, and South and Sgr B2 Main, North, and South. IC 133 West was not initially detected in the first-epoch images because of the reduced sensitivity of the observations. However, reexamination of those images has revealed a corresponding feature that lies in IC 133 West.

Emission from IC 133 Main and from IC 133 West covers distinct velocity ranges and is not distributed evenly throughout the spectrum (Fig. 2). Based on their angular separation and velocities, it is likely that these two centers of activity have separate energetic and dynamic centers. For purposes of this discussion, we have absorbed into IC 133 Main the center of maser activity that was designated IC 133 Southeast by Greenhill et al. (1990), since both are probably associated.

VLBI imaging reveals that many of the strongest maser features evident in the total-power spectrum are superpositions of weaker features. Although only about 50% of the total flux density was recovered by the imaging, the masers are unresolved by our observations. The missing flux density is evident on all baselines, the shortest of which are sensitive to extended structure up to about 3 mas in size (0.01 pc). The missing flux density may arise from weak (< 50 mJy) or far-flung features undetected by the survey of the region, or from destructive interference of emission from features clustered tightly in position and radial velocity.

5. DISCUSSION

5.1. *Proper Motions*

We have measured the first proper motions for an extragalactic H_2O maser source. Ten of the 15 spatially distinct maser features identified in the first epoch images of IC 133 also appear in the second epoch images, 479 days later. As would be expected, given the noted similarity between IC 133 and the strongest Galactic maser sources, the lifetimes of many

TABLE 2

RELATIVE POSITIONS OF H_2O MASER FEATURES AT SECOND EPOCH

Feature	V_{LSR}[a] (km s^{-1})	Band Number[b]	Peak F_ν (mJy)	$\Delta\alpha$[c] (mas)	$\sigma_{\Delta\alpha}$ (mas)	$\Delta\delta$[c] (mas)	$\sigma_{\Delta\delta}$ (mas)	Feature Width[d] (channels)	Integrated Luminosity[e] (10^{-3} $L_\odot$)
IC 133 Main:									
1	−206.88	1	128	0.729	0.003	0.302	0.011	7	3.8
16	−208.10	1	61	−0.162	0.016	0.757	0.026	3	1.0
17	−208.16	1	68	−3.318	0.008	−2.963	0.023	3	0.8
4	−208.84	1	44	−2.843	0.016	−0.997	0.031	2	0.5
19	−209.65	1	826	−0.001	0.002	0.000	0.007	4	11.4
6	−211.33	1	360	0.079	0.009	0.015	0.008	3	4.4
8	−212.13	1	90	−3.284	0.007	−2.186	0.028	2	0.8
9	−213.52	1	141	−2.860	0.003	−0.970	0.015	8	4.9
20	−216.49	1	73	−0.086	0.005	−0.118	0.023	6	1.9
10	−216.63	1	61	−2.906	0.010	−0.597	0.025	5	1.4
11	−218.41	1	162	23.618	0.004	−15.208	0.012	8	4.7
22	−218.44	1	31	−2.619	0.011	−2.404	0.041	2	0.4
23	−218.80	1	75	23.933	0.006	−14.993	0.036	4	1.3
13	−220.23	1	282	−2.596	0.022	0.246	0.012	7	6.7
21	−220.56	1	38	−2.284	0.012	0.431	0.041	3	0.6
14	−222.49	1	77	27.932	0.009	−11.126	0.028	3	1.0
24	−222.81	1	41	23.915	0.011	−14.931	0.043	4	0.8
25	−222.83	1	33	23.620	0.013	−15.259	0.047	4	0.7
26	−224.84	1	51	−2.365	0.010	0.234	0.046	3	0.7
27	−229.22	1	37	22.993	0.010	−15.618	0.038	3	0.6
36	−243.47	2	45	23.638	0.016	−15.230	0.039	2	0.5
IC 133 West:									
15	−222.44	1	119	−288.813	0.008	−40.341	0.032	3	1.5
28	−230.93	2	25	−289.957	0.013	−40.199	0.048	2	0.3
29	−231.10	2	136	−288.790	0.008	−45.370	0.017	4	1.9
30	−231.46	2	36	−289.482	0.013	−38.669	0.048	2	0.4
31	−233.35	2	32	−289.199	0.016	−45.198	0.060	2	0.3
32	−234.35	2	45	−289.443	0.014	−38.835	0.052	2	0.5
33	−235.82	2	33	−289.270	0.015	−45.023	0.056	2	0.3
34	−241.16	2	132	−289.787	0.004	−39.472	0.016	4	3.1
35	−243.92	2	70	−289.776	0.007	−39.245	0.049	4	1.5
37	−246.91	2	31	−289.484	0.016	−39.101	0.066	2	0.3
38	−253.47	3	89	−289.786	0.009	−39.487	0.020	8	2.8

[a] Mean velocities of features, weighted by flux density, with respect to the local standard of rest. To obtain heliocentric velocities, add +0.52 km s^{-1}.

[b] Band 1 contains the reference feature and is centered at V_{LSR} = −216.28 km s^{-1}. Bands 2 and 3 are centered at V_{LSR} = −240.35 and −264.43 km s^{-1}, respectively (see § 2).

[c] The relative position for each feature is the weighted average of positions measured in the contributing channel maps, corrected to epoch J2000. Features 28 through 37 lie in a "remote" band. For them the origin of coordinates is uncertain by an additional 11 and 49 μas ($\sigma_{\Delta\alpha}$, $\sigma_{\Delta\delta}$; see § 3). The same is true for feature 38, which lies in a separate band. The reference position is $\alpha_{2000} = 01^h33^m16^s.545 \pm 0^s.008$, $\delta_{2000} = 30°52'50''.0 \pm 0''.1$.

[d] Each channel is 0.48 km s^{-1} wide.

[e] Luminosities of the features integrated across the line profiles, assuming isotropic emission of radiation.

of the maser features exceed 1 yr. Reliable motions can be estimated in right ascension for five of the 10 features detected at both epochs (see Table 3). Figure 3 shows the motion associated with each frequency channel that contributes to the five features. The measurement of proper motions in IC 133 requires relative position accuracies to be $\lesssim 10$ μas. Motions in declination could not be measured as accurately since the interferometer beam is about 4 times larger in declination than in right ascension, making the positional accuracies from the first epoch observations inadequate.

The requisite positional accuracy is achieved by measuring the positions of the masers to a fraction of the beamwidth, which is possible because of the high SNR of the synthesized images. However, unresolved source structure can cause significant biases and the actual accuracy of the positions may be less than the precision inferred from the SNR (see Reid 1991). To illustrate this effect, we note that the smallest interferometer beams obtainable using ground-based arrays operating at 1.3 cm wavelength are about 200 μas, which corresponds to a

TABLE 3

PROPER MOTIONS OF IC 133 H_2O MASER FEATURES

Feature Designation[a]	V_{LSR}[b] (km s^{-1})	$\Delta\theta_\alpha$[c] (μas)	$\sigma_{\Delta\theta_\alpha}$ (μas)	$\Delta\theta_\delta$[c] (μas)	$\sigma_{\Delta\theta_\delta}$ (μas)
1	−206.88	7.8	6.9	104	31
6	−211.33	−14	6.5	−6.7	8.6
11	−218.41	10.	10.	−52	45
14	−222.49	17	16	52	73
15[d]	−222.44	1.9	13	96	59

[a] Nomenclature for both first and second epochs.

[b] Mean velocities for the maser features at the second epoch.

[c] Proper motions in the sense epoch 2 minus epoch 1. The weighted mean motion of 86.5 μas and 33.8 μas in right ascension and declination has been removed. This corrects the motions for the different positions of the reference features at the two epochs, and for their motions with respect to the rest of masers in IC 133 Main. The weighted mean was computed excluding feature 15, which lies in IC 133 West (see § 5.2). If feature 15 is included then the weighted mean motion increases by 0.2 and 1.8 μas in right ascension and declination, respectively.

[d] Feature lies in IC 133 West.

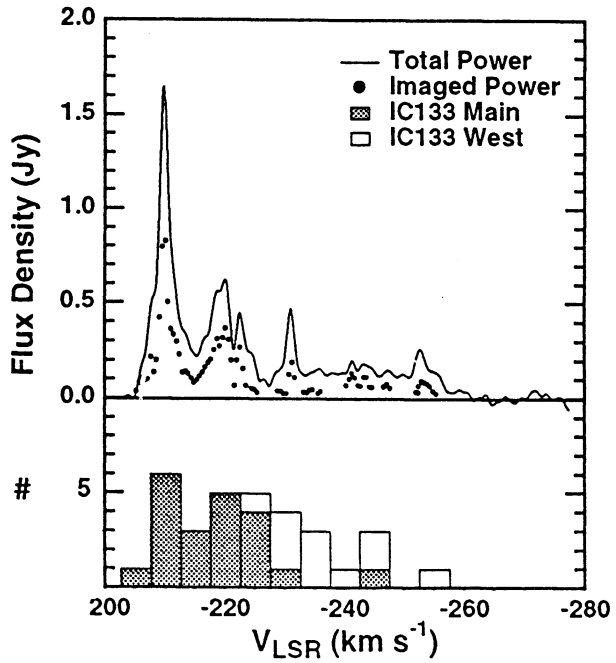

FIG. 2.—Total power spectrum (*solid line*) of the IC 133 maser made with 3.6 hr of VLBI autocorrelation data from MPI. A spectrum displaying the power recovered by the synthesis imaging is overlayed (*crosses*). A histogram of the radial velocities of maser features appears below.

linear distance of $\sim 2 \times 10^{15}$ cm at M33. This dimension is similar to the scale size of the regions on which maser features cluster together in Galactic sources. Toward W49N, Gwinn et al. (1989) found maser clusters that contain several maser components at similar velocities and that are separated by less than 5×10^{15} cm. For the smaller clusters, the structure would be unresolved (the features "blended") and changes in the relative flux densities of the component features, between two epochs, would mimic proper motions.

We used three conditions to evaluate the "reliability" of the proper motions attached to each maser feature observed at the two epochs. First, the line profile must be substantially the same at each epoch. Second, the profiles must be centrally peaked at the same LSR velocity (to within one spectral channel) at each epoch. Third, both the line profiles and brightness distributions of overlapping features must be clearly separable. To further reduce the effects of blending, the computed motions for each feature were the weighted average of the motions for the individual constituent frequency channels, and mainly those near line center (see Fig. 3).

Lacking a third-epoch observation, we cannot test whether the apparent proper motions actually indicate straight-line trajectories, as expected. Hence, despite the care taken in data analysis, blending cannot be entirely discounted as the cause of the reported motions. Note that ersatz motions caused by interstellar scintillation in our Galaxy are expected to be small, less than 2 μas at the Galactic latitude of M33 (Cordes 1984). Significant interstellar scintillation in M33 is also unlikely because the interfering plasma is so close to the maser source.

The reference features at the two epochs were chosen independently to optimize the SNR of the respective images. By late 1988, the reference feature of the first epoch was no longer strong enough to be used, and the second epoch reference feature was not detectable in the first epoch data. Hence, we subtracted the weighted mean motions in right ascension and in declination from the gross motions presented in Figure 3. The consequences (i.e. second-order effects) of choosing different reference features at different epochs are negligible since the

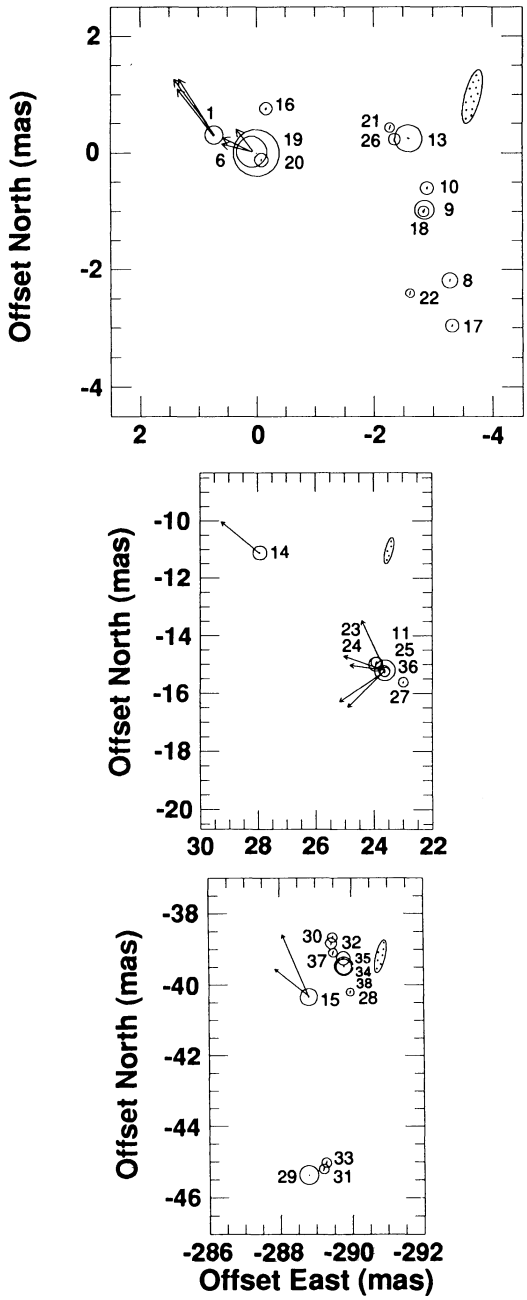

FIG. 3.—*Top:* The northwestern component of IC 133 Main. *Center:* The southeastern component of IC 133 Main. *Bottom:* IC 133 West. The center and bottom images have equal plate scales. Each circle corresponds to a distinct maser feature and the area is proportional to the peak flux density. The maser features are numbered to indicate the corresponding spectral features, as enumerated in Table 2. Error bars for the positions appear at the center of each circle but may not be visible for the stronger features. Arrows indicate the gross proper motions between the two epochs. For each feature, motions are shown for each contributing frequency channel. The arrow attached to feature 14 corresponds to a motion of 134 μas. Only the motions in right ascension are meaningful, owing to the much larger measurement errors in declination. The FWHM of the synthesized beam is shown in the northwest corner of each map.

two features are separated by only about 80 μas and are only 1 km s^{-1} apart in the spectrum.

5.2. *Interpretation of Proper Motions*

Distances may be estimated from proper motion measurements by two techniques (Genzel et al. 1981a). Sources that have systematic streaming motions, such as spherically symmetric outflow, may be fit by a dynamical model in which distance is one of the parameters in the solution (e.g., Sgr B2N in Reid et al. 1988). A simpler and less general parallax technique, statistical parallax (cf. Trumpler and Weaver 1953), is appropriate for sources in which the observed three-dimensional maser motions are isotropic and possibly random. Distances estimated by statistical parallax (the quotient of the dispersions in radial Doppler motions and in transverse angular motions) can be biased by common astronomical phenomena, such as nonisotropic streaming motions or beaming of maser radiation.

The sparse sampling of proper motions in IC 133 makes meaningful analysis by model fitting impossible. Although the dynamics within IC 133 cannot be ascertained without independent measurements, statistical parallax does offer a rudimentary check as to whether the measured proper motions are consistent with conventional distance estimates for M33. Analysis of proper motions in W51 (Genzel et al. 1981b; Schneps et al. 1981) relied upon statistical parallax.

Measurement errors in the proper motions, if unaccounted for, increase the dispersion in apparent transverse motions. In the M33 data the measurement errors are not only significant but vary with the signal strength of the maser feature. If the underlying or true dispersion is σ_T and the measurement errors are σ_{mi}, then the maximum likelihood estimator of σ_T is given by the solution to the equation

$$\sum_i^N \frac{(\sigma_{mi}^2 + \sigma_T^2) - (x_i - m)^2}{(\sigma_{mi}^2 + \sigma_T^2)^2} = 0 , \quad (1)$$

where the x_i is the measured proper motion of the ith feature and m is the true (weighted) mean of the distribution. The solution to this equation in the case where the measurement errors are the same, σ_m, reduces to the expression given by Genzel et al. (1981a),

$$\sigma_T = \frac{1}{N}\sum_i^N (x_i - m)^2 - \sigma_m^2 . \quad (2)$$

We have solved equation (1) iteratively using the data in Table 3 for the motions in right ascension. We used the weighted mean motions listed in Table 3 for values of m. For the four features in IC 133 Main, we find $\sigma_T = 8.3$ μas (motion over 479 days). Since the apparent rms dispersion (σ_A) in transverse motions is 11.7 μas, we calculate an effective measurement error (σ_M) of 8.2 μas. Including feature 15 from IC 133 West in the analysis, we obtain $\sigma_T = 7.4$ μas and $\sigma_A = 11.2$ μas.

The dispersion in radial velocities depends upon a priori assumptions about the dynamics in the IC 133 region. The shape of the total-power spectrum, with all the emission to one side of the strongest peak at $V_{LSR} \sim -210$ km s^{-1}, is not indicative of isotropic motions (cf. W51M; Genzel et al. 1981b). Coincidently, the measured systematic H I velocity for the region is also -210 ± 4 km s^{-1} (Rogstad, Wright, & Lockhart 1976; 2′ resolution). However, with a 21″ beam positioned within 2″ of the maser, Israel (1991) observed spatially unresolved CO ($J = 2 \rightarrow 1$) emission at -220 ± 2 km s^{-1}. This velocity is between the mean velocities of IC 133 Main and IC 133 West. If -210 km s^{-1} is the systematic radial velocity of IC 133 Main and IC 133 West is dynamically unrelated, then the dispersion in radial velocities for IC 133 Main is 11.5 km s^{-1}. If features from IC 133 West are included, then the dispersion is 18.9 km s^{-1}. If the systematic velocity is as low as -205 km s^{-1} (the absolute redward limit of maser emission) the dispersions increase to 15.3 and 21.6 km s^{-1}, respectively. The range of possible dispersions, 11.5–21.6 km s^{-1}, corresponds to an angular velocity range of 4.4–8.4 μas over 479 days. We adopt a value of 7.8 μas for the transverse dispersion, σ_T, and a value of 6.4 μas for the equivalent radial velocity dispersion, σ_R. This suggests a distance ($720\sigma_R/\sigma_T$) of $\sim$600 kpc, although it is more a measure of consistency than a formal estimate of distance.

The statistical error in the distance estimate, divided by the distance, is given approximately by the equation (Genzel et al. 1981a)

$$\frac{\sigma_D}{D} = \left\{\frac{1}{2N[1 - (\sigma_M/\sigma_A)^2]}\right\}^{1/2} , \quad (3)$$

where N is the number of maser features. For $N = 5$, $\sigma_M = 8.0$ and $\sigma_A = 11.3$, we obtain $\sigma_D/D \sim 0.45$. Note that the contribution to this error due to the finite sample size is 0.31. Finally, we estimate the systematic error to be 0.25, which is dominated by the uncertainty in the systematic velocity of the region and in the relationship between IC 133 Main and IC 133 West. Combining the statistical and systematic errors in quadrature gives a total fractional error in distance of 0.50 or about 300 kpc. As a final caution, we note that the result depends strongly on feature 6, the only feature whose motion clearly exceeds the noise level. It is possible that if the feature contains multiple spatially distinct components at the same velocity the time variations in their intensity could mimic proper motion (see § 5.1). Such an effect would increase the measured dispersion in angular velocity and decrease the estimated distance.

We have interpreted the motions in IC 133 to be of kinematic origin, rather than artifacts caused by unseen structure and fluctuations in the brightness of the unresolved components between epochs. In four of the six proper motion studies of Galactic maser sources, the linear motions of masers were tracked over three or more epochs, which greatly reduced the probability that the apparent motions were a manifestation of such "Christmas tree" effects. In the future, additional epochs of observation will be available, and if more features are found, model fitting will be possible.

6. SUMMARY

We have demonstrated the feasibility of measuring the relative positions of weak extragalactic H_2O maser features with accuracies of better than 10 μas, approximately the statistical noise limit for existing ground-based instruments. A second center of maser activity has been discovered, IC 133 West, which is displaced $\approx$0.″3 (1 pc at 720 kpc) from the previously observed center, IC 133 Main. The average radial velocity of the maser features in IC 133 West is blueshifted with respect to that of IC 133 Main by about 20 km s^{-1}.

By comparing images from two epochs separated by 479 days, we have assembled a sample of proper motions in right ascension that is roughly consistent with the distribution of line-of-sight velocities, for the accepted distance to M33 of 720 kpc. The sample of motions admits a fractional uncertainty in

distance of 50%. The ambiguous relationship between IC 133 Main and IC 133 West, uncertainty in the systematic velocity of the region, and small sample of proper motions are the major sources of uncertainty in estimating distance. Subsequent VLBI observations will permit the tracking of proper motions over more than two epochs, establishing the motions as kinematic in nature and enlarging the sample of proper motions sufficiently that modeling may provide a useful estimate of the distance to M33. Supplementary observations, such as high-resolution spectroscopy of Hα emission, will be needed to measure the systematic velocity of the region.

The diligent efforts of the six observatory staffs during the data acquisition beginning in 1987 are very much appreciated. We are especially grateful to the scientific and Mark III correlator personnel at Haystack Observatory. This work forms part of the Ph.D. dissertation at Harvard University of L. J. G., who was supported by the NASA Graduate Student Researchers Program, and later supported as a Research Fellow by the Miller Institute for Basic Research in Science, University of California, Berkeley, CA.

REFERENCES

Cordes, J. M. 1984, in IAU Symp. 110, VLBI and Compact Radio Sources, ed. R. Fanti, K. Kellermann, & G. Setti (Dordrecht: Reidel), 303
Genzel, R., Reid, M. J., Moran, J. M., & Downes, D. 1981a, ApJ, 244, 884
Genzel, R., et al. 1981b, ApJ, 247, 1039
Greenhill, L. J. 1990, Ph.D. thesis, Harvard
Greenhill, L. J., Moran, J. M., Reid, M. J., Gwinn, C. R., Menten, K. M., Eckart, A., & Hirabayashi, H. 1990, ApJ, 364, 513
Gwinn, C. R., Moran, J. M., Reid, M. J., Schneps, M. H., Genzel, R., & Downes, D. 1989, in IAU Symp. 136, The Center of the Galaxy, ed. M. Morris (Dordrecht: Kluwer), 47
Israel, F. P. 1991, private communication
Israel, F. P., Hawarden, T. G., Geballe, T. R., & Wade, R. 1990, MNRAS, 242, 471
Reid, M. J. 1991, in Adv. Space Res., 11, 421
Reid, M. J., Gwinn, C. R., Moran, J. M., & Matthews, A. H. 1988, BAAS, 20, 1017
Reid, M. J., & Moran, J. M. 1988, in Galactic and Extragalactic Radio Astronomy, ed. G. L. Verschuur & K. I. Kellermann (2d ed.; New York: Springer-Verlag), chap. 6
Reid, M. J., Moran, J. M., & Gwinn, C. R. 1987, in Radio Astronomy in Space: Proc. Green Bank Workshop, ed. K. Wieler (Charlottesville: NRAO), 141
Rice, W., Boulanger, F., Viallefond, F., Soifer, B. T., & Freedman, W. L. 1990, ApJ, 358, 418
Rogstad, D. H., Wright, M. C. H., & Lockart, I. A. 1976, ApJ, 204, 703
Schneps, M. H., Lane, A. P., Downes, D., Moran, J. M., Genzel, R., & Reid, M. J. 1981, ApJ, 249, 124
Thompson, A. R., Moran, J. M., & Swenson, G. W. 1986, Interferometry and Synthesis in Radio Astronomy (New York: Wiley–Interscience)
Trumpler, R. J., & Weaver, H. F. 1953, Statistical Asytronomy (New York: Dover)
Walker, R. C., Matsakis, D. N., & Garcia-Barreto, J. A. 1982, ApJ, 255, 128